Quantum phase transition in a coupled two-level system embedded in anisotropic three-dimensional photonic crystals

H. Z. Shen,[1,2,3] X. Q. Shao,[1,2] G. C. Wang,[1,2] X. L. Zhao,[1,3] and X. X. Yi[1,2,*]

[1]*Center for Quantum Sciences and School of Physics, Northeast Normal University, Changchun 130024, China*

[2]*Center for Advanced Optoelectronic Functional Materials Research, and Key Laboratory for UV Light-Emitting Materials and Technology of Ministry of Education, Northeast Normal University, Changchun 130024, China*

[3]*School of Physics and Optoelectronic Technology, Dalian University of Technology, Dalian 116024, China*

(Received 17 July 2015; revised manuscript received 2 November 2015; published 7 January 2016)

The quantum phase transition (QPT) describes a sudden qualitative change of the macroscopic properties mapped from the eigenspectrum of a quantum many-body system. It has been studied intensively in quantum systems with the spin-boson model, but it has barely been explored for systems in coupled spin-boson models. In this paper, we study the QPT with coupled spin-boson models consisting of coupled two-level atoms embedded in three-dimensional anisotropic photonic crystals. The dynamics of the system is derived exactly by means of the Laplace transform method, which has been proven to be equivalent to the dissipationless non-Markovian dynamics. Drawing on methods for analyzing the ground state, we obtain the phase diagrams through two exact critical equations and two QPTs are found: one QPT is that from the phase without one bound state to the phase with one bound state and another is that from one phase with the bound state having one eigenvalue to another phase where the bound state has two eigenvalues. Our analytical results also suggest a way of control to overcome the effect of decoherence by engineering the spectrum of the reservoirs to approach the non-Markovian regime and to form the bound state of the whole system for quantum devices and quantum statistics.

DOI: 10.1103/PhysRevE.93.012107

I. INTRODUCTION

It is exploitable to effectively describe many realistic situations, and a two-level system (TLS) [1–3] coupled to a bath of bosonic modes is of great significance. Despite its simplicity, the system reveals a multifaceted behavior in statics, dynamics, and quantum criticality, for which it becomes a paradigmatic model in the field of quantum dissipation. The theoretical analysis as well as the practical implementation of two-level systems thus represents a central topic in several branches of modern physics ranging from high-energy to nuclear and condensed matter physics [4–10].

The quantum phase transition (QPT) [11] based on TLSs has attracted considerable attention within various fields of physics in recent years. They have been studied in condensed-matter physics because they provide valuable information about the novel type of zero-temperature states of matter that emerge in the vicinity of QPTs, which occur at zero temperature and are driven by purely quantum effects. In the parameter space, the points of nonanalyticity of the ground-state energy density are referred to as *critical points* and they define the QPTs. The QPT describes a sudden qualitative change of the macroscopic properties mapped from the eigenspectrum of a quantum many-body system [11]. One of the motivations is that the exploration of the QPT in the TLS could result in some insight into the decoherence control of systems. QPTs have been intensively studied for quantum systems subject to the environment [12–19]. These phenomena happen when some kinds of nonanalytic behavior [20,21] arise in an excited region of the energy spectrum, normally a singularity in the density of states or in the flow of the energy spectrum through the critical energy line. To the present, many methods have been explored to investigate the QPTs, such as unitary transform [22–25], the path-integral method [4], the quantum Monte Carlo method [26], the numerical renormalization-group method [27,28], and numerical diagonalization in a coherent-state basis [12]. Subsequently, a sequence of experimental groups have observed the reservoir-induced QPT by employing mesoscopic metal rings [29], cold atoms in optical lattices [30,31], as well as single-electron transistors with electromagnetic noise [32,33].

Many explorations of quantum phase transition are mainly based on the physics with the spin-boson model, where the delocalized regime exhibits many interesting phenomena. For example, it was found that an eigenstate with one real eigenvalue for atom plus environment shows the system possesses a bound state [34–37]. Nevertheless, the understanding of this dynamical transition and the physics in the regime of finite coupling strength between two coupled spin-boson models have not been clear so far.

For this purpose, we study quantum phase transition with coupled spin-boson models consisting of coupled two-level atoms embedded in three-dimensional anisotropic photonic crystals. The ground-state property of the system is obtained analytically with and without the rotating wave approximation (RWA), respectively. Under the RWA, our starting point is to examine whether bound states exist between two two-level atoms in a three-dimensional anisotropic photonic crystal. Two critical equations for three phases are exactly derived and we analytically give the formulas of the energy spectrum for the whole system including system-plus-environment. Two typical QPTs occur in our system, and different ground states are associated with three phases that we label (I)–(III), which correspond to a zero-exciton eigenstate, a bound state with a real eigenvalue, and a bound state with two real eigenvalues, respectively. The first QPT occurs between phases I and II. The existence of the second QPT originates from the transition of

*yixx@nenu.edu.cn

two bound states II and III. This novel bound state shows the period oscillation behavior for the system, which arises from the quantum interference of two localized modes. When the non-RWA is applied, we show that the similar QPT still exists in the delocalized phase regime, where the renormalized factors take finite values by enjoying the perturbation approach to neglect the high-order interaction terms in a unitarily transformed Hamiltonian. The approximation is justified by the fact that the high-order excitations are negligible in the weak-coupling regime. Also, one can verify that the neglected terms give no contribution to the QPT we obtained, which validates our approximations.

The remainder of the paper is organized as follows. In Sec. II, we introduce a general model to describe the coupled spin-boson models consisting of two coupled two-level atoms embedded in three-dimensional anisotropic photonic crystals and derive the exact Dyson equation. In Sec. III, we give the exact solution of the system dynamics. In Sec. IV, we analyze the structure of roots for Green function $G(s)$ and exactly derive two critical equations. In Sec. V, we analyze the phase diagrams. In Sec. VI, we discuss the time evolution and long-time behavior of the population and correlation corresponding to three phases, respectively. In Sec. VII, we study ground-state fidelity and entanglement entropy to further confirm the existence of the quantum phase transitions. Section VIII is devoted to the study of the quantum phase transition without rotating wave approximation by means of pertubation approach based on a unitary transform. Discussion and conclusions are given in Sec. IX.

II. EXACT TIME EVOLUTION FOR THE SYSTEM DYNAMICS

A. The model

We now consider two coupled spin-boson models consisting of two-level atoms, with atomic levels $|e\rangle$ and $|g\rangle$ and eigenfrequencies ω_a and ω_b, respectively, embedded in a three-dimensional anisotropic photonic crystal, as shown in Fig. 1. The two atoms are assumed to be near the edge of a photonic band gap with frequency ω_e. An interesting problem in this type of system is the decoherence resulting from the influence of an environment, which is usually represented by an infinite set of harmonic oscillators. The coupled spin-boson models without RWA take

$$\hat{H} = \hat{H}_a + \hat{H}_b + \hat{H}_{ab}, \tag{1}$$

with

$$\hat{H}_m = \hbar\omega_m \sigma_m^+ \sigma_m^- + \sum_k \left[\hbar V_{m,k} \sigma_m^x (\hat{b}_{m,k} + \hat{b}_{m,k}^\dagger)\right] + \sum_k \hbar\omega_{m,k} \hat{b}_{m,k}^\dagger \hat{b}_{m,k}, \tag{2}$$

$$\hat{H}_{ab} = \hbar J \sigma_a^x \sigma_b^x,$$

where $m = a,b$; $\sigma^- = |g\rangle\langle e|$ is Pauli matrix; $|e\rangle$ and $|g\rangle$ represent the excited and ground states of the qubit, respectively; and $\sigma_m^x = \sigma_m^- + \sigma_m^+$. H.c. denotes the Hermitian conjugate. $\hat{b}_{m,k}$ ($\hat{b}_{m,k}^\dagger$) is the annihilation (creation) operator for the k-th reservoir mode with frequency $\omega_{m,k}$ for m-th atom, and $V_{m,k}$ the coupling strength between the m-th atom and the k-th electromagnetic mode. The detailed evolution of J as a function of atomic distance R for a typical anisotropic photonic band gap can be found in Refs. [38,39]. Since our model is very close to the edge of the band gap, $V_{m,k}$ can be approximated to [40]

$$V_{m,k} = (\omega_m d_m/\hbar)\sqrt{\hbar/(2\varepsilon_0 \omega_{m,k} V)}\vec{e}_{m,k} \cdot \vec{u}_m, \tag{3}$$

where k represents both the momentum and the polarization of the modes. d_m and $\vec{u}_m$ are the magnitude and unit vector of the atomic dipole moment of the transition, respectively. V is the quantization volume, $\vec{e}_{m,k}$ are the transverse unit vectors for the reservoir modes, and ε_0 is the vacuum dielectric constant. If a three-dimensional anisotropic photonic crystal has an allowed point-group symmetry, then the dispersion relation near the band edge could be expressed approximately with [41]

$$\omega_{m,k} = \omega_e + B_m |\vec{k} - \vec{k}_0^j|^2, \tag{4}$$

where ω_e is the cut-off frequency of the band edge. k_0^j are the finite collections of symmetry related points, which are associated with the band edge. B_m is the model-dependent constant. The corresponding state density is $\rho(\omega) \propto (\omega - \omega_e)^{1/2}\theta(\omega - \omega_e)$ [37,38] [see Fig. 2(a)], and here θ is step function. Figures 2(b) and 2(d) will be discussed in Sec. V.

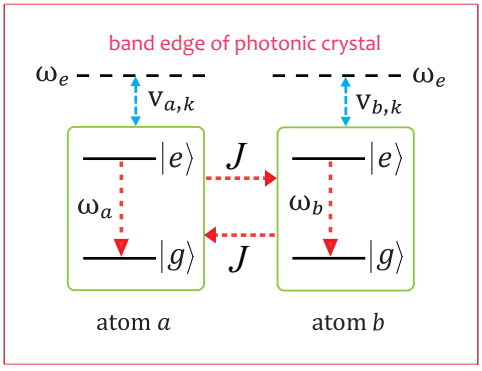

FIG. 1. (a) The scheme of two two-level atoms embedded in photonic crystals with the counter-rotating terms.

B. Exact dynamics for the system under RWA

The interaction Hamiltonian in Eq. (1) contains the counter-rotating terms $\hat{b}_{m,k}\sigma_m^-$ and $\hat{b}_{m,k}^\dagger\sigma_m^+$. A used approximation in quantum optics and quantum information communities is the RWA, which is valid in the weak-coupling limit. Then, in this condition, Eq. (1) can be written as

$$\hat{H}^{\mathrm{RWA}} = \hat{H}_a^{\mathrm{RWA}} + \hat{H}_b^{\mathrm{RWA}} + \hat{H}_{ab}^{\mathrm{RWA}}, \tag{5}$$

with

$$\hat{H}_m^{\mathrm{RWA}} = \hbar\omega_m \sigma_m^+ \sigma_m^- + \sum_k [\hbar V_{m,k} \hat{b}_{m,k} \sigma_m^+ + \mathrm{H.c.}] + \sum_k \hbar\omega_{m,k} \hat{b}_{m,k}^\dagger \hat{b}_{m,k}, \tag{6}$$

$$\hat{H}_{ab}^{\mathrm{RWA}} = \hbar J \sigma_a^+ \sigma_b^- + \hbar J \sigma_a^- \sigma_b^+,$$

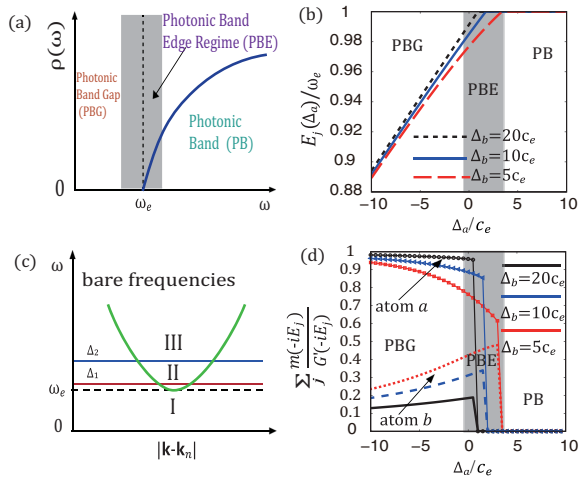

FIG. 2. Band structures of photonic crystals and localized photon modes. (a) The state density $\rho(\omega)$ of the two-level atoms coupled to photonic crystals. The spectrum is divided into three regimes: photonic band gap (PBG), the vicinity of the photonic band edge (PBE), and the photonic band (PB). (b) The corresponding localized photon mode eigenfrequency E_j given by Eq. (31) as a function of the detuning $\Delta_a = \omega_a - \omega_e$, and (d) the corresponding localized photon mode amplitudes, given in Eqs. (17) and (18). Other parameters chosen are $\omega_e = 100c_e, J = 4c_e$, where c_e is given by Eq. (13). (c) Frequency regimes in a photonic crystal. For frequency detunings, Δ_a from the band edge ω_e with $\Delta_a < \Delta_1$, (region I), the atom frequency lies in the forbidden band. For $\Delta_1 < \Delta_a < \Delta_2$ (region II), the atom frequency is exactly at the band edge, and $\Delta_a > \Delta_2$ (region III) the atom frequency stays in the allowed band.

Hamiltonian (5) is analytically solvable due to the total excitation number N in Eq. (A1) is conserved. For simplicity, we initially prepare the two atoms in a linear superposition of states with one exciton

$$|\psi(0)\rangle = [A_a(0)|eg\rangle + A_b(0)|ge\rangle] * |0_k\rangle_a|0_k\rangle_b, \tag{7}$$

with $|A_a(0)|^2 + |A_b(0)|^2 = 1$. In order to study the ground-state properties of the system, we derive the retarded Green function at zero temperature, which can be defined by [42,43]

$$\mathcal{U}_{mn}(t-t') = -i\theta(t-t')\langle\{\sigma_m^-(t),\sigma_n^+(t')\}\rangle, \tag{8}$$

where $\langle\cdot\rangle$ denotes expectation value with the initial state (7) and $\{\cdot\}$ the anticommutation relation.

Taking the initial time $t' = 0$ and considering Eq. (A2), we obtain the matrix form of the Green function,

$$\mathcal{U}(t) = \begin{bmatrix} -iA_a(0)^*A_a(t) & -iA_b(0)^*A_a(t) \\ -iA_a(0)^*A_b(t) & -iA_b(0)^*A_b(t) \end{bmatrix}, \tag{9}$$

which can be fully determined by the Dyson equation,

$$\dot{\mathcal{U}}(t) + i\mathbf{M}\mathcal{U}(t) + \int_0^t d\tau \mathcal{F}(t-\tau)\mathcal{U}(\tau) = 0, \tag{10}$$

where the other coefficients $\mathbf{M} = \begin{pmatrix} \omega_a & J \\ J & \omega_b \end{pmatrix}$, $\mathcal{F}(t) = \begin{pmatrix} f_a(t) & 0 \\ 0 & f_b(t) \end{pmatrix}$. The exact Green function equation (10) can be solved by means of a Laplace transform in the frequency domain. For more detailed derivations of Eq. (10), see Appendix A. The Dyson equation (10) characterizes all the back-actions between the atoms and photonic crystals and can be determined uniquely by the coupled strength $|V_{m,k}|^2$ between atoms and photonic crystals through the fluctuation dissipation relation (A5).

III. THE EXACT SOLUTION OF THE SYSTEM DYNAMICS

To investigate excitation state evolutions in photonic crystal [44–50], we must first solve the dynamics of photon determined by Eq. (10). We proceed to make use of Laplace transform $X(s) = \int_0^\infty X(t)e^{-st}dt$ [51–54] and obtain from Eq. (10)

$$\begin{aligned} A_a(s) &= \frac{-iA_b(0)J + A_a(0)[s + i\omega_b + f_b(s)]}{J^2 + [s + i\omega_a + f_a(s)][s + i\omega_b + f_b(s)]}, \\ A_b(s) &= \frac{-iA_a(0)J + A_b(0)[s + i\omega_a + f_a(s)]}{J^2 + [s + i\omega_a + f_a(s)][s + i\omega_b + f_b(s)]}, \end{aligned} \tag{11}$$

where

$$f_m(s) = \sum_k \frac{|V_{m,k}|^2}{s + i\omega_{m,k}}. \tag{12}$$

Using the dispersion relation (4), and converting the mode sum over transverse plane waves into an integral and performing the integral (see Appendix B), we have

$$f_m(s) = \frac{-ic_e}{\sqrt{\omega_e} + \sqrt{-is + \omega_e}}, \tag{13}$$

where we have assumed $c_a = c_b \equiv c_e$ with $c_m = (\omega_m d_m)^2 \sum_{j_1} \sin^2(\theta_{j_1})/(8\pi\varepsilon_0\hbar B_m^{3/2})$ $(m = a,b)$ because we can make the atomic dipole moments of two transitions parallel to each other and appropriately adjust the magnitude d_m and B_m and make $V_{a,k} = V_{b,k} = V_k$. Therefore we set $f_a(s) = f_b(s)$ for the sake of simplicity. Here θ_{j_1} is the angle between the dipole vector of the atom and the j-th k_0^j. The phase angle of s is defined by $-\pi < \arg(s) < \pi$, and the phase angle of $\sqrt{-is + \omega_e}$ in $f_m(s)$ is defined by $-\frac{\pi}{2} < \arg\sqrt{-is + \omega_e} < \frac{\pi}{2}$. The amplitudes $A_a(t)$ and $A_b(t)$ can then be obtained by means of a inverse Laplace transform

$$A_m(t) = \frac{1}{2\pi i}\int_{\sigma-i\infty}^{\sigma+i\infty} A_m(s)e^{st}ds, \tag{14}$$

where the real number σ is conditionally chosen so $s = \sigma$ lies to the right of all the singularities (poles and branch points) of functions $A_a(s)$ and $A_b(s)$. With the help of complex function integration and the residue theorem, we can obtain the expression of the amplitudes:

$$\begin{aligned} A_a(t) = &\sum_j \frac{m_1(x_j^{(1)})e^{x_j^{(1)}t}}{G'(x_j^{(1)})} + \sum_j \frac{m_2(x_j^{(2)})e^{x_j^{(2)}t}}{L'(x_j^{(2)})} \\ &+ \frac{1}{2\pi i}\int_0^\infty dy\lambda_a(-y - i\omega_e)e^{-yt - i\omega_e t}, \end{aligned} \tag{15}$$

$$\begin{aligned} A_b(t) = &\sum_j \frac{m_3(x_j^{(1)})e^{x_j^{(1)}t}}{G'(x_j^{(1)})} + \sum_j \frac{m_4(x_j^{(2)})e^{x_j^{(2)}t}}{L'(x_j^{(2)})} \\ &+ \frac{1}{2\pi i}\int_0^\infty dy\lambda_b(-y - i\omega_e)e^{-yt - i\omega_e t}, \end{aligned} \tag{16}$$

where $\lambda_a(s) = \frac{m_2(s)}{L(s)} - \frac{m_1(s)}{G(s)}$ and $\lambda_b(s) = \frac{m_4(s)}{L(s)} - \frac{m_3(s)}{G(s)}$. The other functions $m_1(s)$, $m_2(s)$, $m_3(s)$, $m_4(s)$, $G(s)$, and $L(s)$ in Eqs. (15) and (16) are defined in Appendix C. Detailed derivations of Eqs. (15) and (16) are given in Appendix C. $x_j^{(1)}$ are the roots of equation $G(s) = 0$ in region [$\mathrm{Re}(s) > 0$ or $\mathrm{Im}(s) > -\omega_e$], and $x_j^{(2)}$ are the roots of $L(s) = 0$ in region [$\mathrm{Re}(s) < 0$ and $\mathrm{Im}(s) < -\omega_e$]. $G'(s)$ and $L'(s)$ are derivatives of those functions $G(s)$ and $L(s)$, respectively.

The first term in (15) and (16) corresponds to localized modes with $s = -iE_j$ (E_j are real numbers, which correspond to the energy spectrum of the whole system). The localized modes exist if and only if the environmental spectral density has band gaps located at the pure imaginary zeros with $G(-iE_j) = 0$. These localized modes do not decay, which give dissipationless non-Markovian dynamics. The nonlocalized mode contains two parts: One is the second term in Eqs. (15) and (16), which is the oscillating damping process due to the complex roots in $L(s) = 0$ in the regime of [$\mathrm{Re}(s) < 0$ and $\mathrm{Im}(s) < -\omega_e$]. The other is the integral part, i.e., the nonexponential parts will oscillate rapidly in time. This rapidly oscillating damping, which originates from the terms containing $e^{i\omega_e t}$ in Eqs. (15) and (16). Therefore the nonlocalized mode parts in (15) and (16) are the contribution of the allowed bands, which usually generate exponential decays. This is another significance of the non-Markovian dynamics.

We show that the probability amplitudes in Eqs. (15) and (16) from the Lebesgue-Riemann lemma [55] in the long-time regime ($t \to \infty$) reach

$$A_a(t \to \infty) = \sum_j \frac{m_1\left(x_j^{(1)}\right) e^{x_j^{(1)} t}}{G'\left(x_j^{(1)}\right)}, \tag{17}$$

$$A_b(t \to \infty) = \sum_j \frac{m_3\left(x_j^{(1)}\right) e^{x_j^{(1)} t}}{G'\left(x_j^{(1)}\right)}. \tag{18}$$

In particular, we notice that the two atoms decouple each other when coupled strength $J = 0$. Therefore, using a method similar to Eq. (15), one can obtain the expression of the amplitude,

$$A_a(t) = \sum_j \frac{A_a(0) e^{u_j^{(1)} t}}{G'_0\left(u_j^{(1)}\right)} + \sum_j \frac{A_a(0) e^{u_j^{(2)} t}}{L'_0\left(u_j^{(2)}\right)} + \frac{1}{2\pi i} \int_0^\infty dy \mu(-y - i\omega_e) e^{-yt - i\omega_e t}, \tag{19}$$

where $G_0(s) = s + i\omega_a - \frac{i}{\sqrt{\omega_e} + \sqrt{-is + \omega_e}}$, $L_0(s) = s + i\omega_a - \frac{i}{\sqrt{\omega_e} - i\sqrt{is - \omega_e}}$, $\mu(s) = A_a(0)[\frac{1}{L_0(s)} - \frac{1}{G_0(s)}]$, and $G'_0(s)$ and $L'_0(s)$ are derivatives of functions $G_0(s)$ and $L_0(s)$. respectively. $u_j^{(1)}$ and $u_j^{(2)}$ are the roots of $G_0(s) = 0$ and $L_0(s) = 0$, respectively. These results are in agreement with earlier studies [40,49,56].

IV. THE STRUCTURE OF ROOTS FOR GREEN FUNCTION

Equations (15) and (16) provide the analytical expressions of the non-Markovian dissipative dynamics in three-dimensional photonic crystal. It shows that the dynamics in PCs always contains two parts: a localized photon mode (the first term) plus a nonexponential photon damping (the terms except the first term). The localized photon mode is a long-lived non-Markovian effect (dissipationless), induced by the PBG structure in PCs. Therefore to study the dissipationless dynamics of the system, we need to obtain the structure of pure imaginary roots for $G(s) = 0$. According to the Green function theory [43], the zero point of the denominator in the frequency domain of the Green function $\mathcal{U}(s)$ corresponds to the energy spectrum of the whole system. In the following, we will confirm this point.

A. Energy spectrum analysis of the Green's function

Here we highlight the Green's function $\mathcal{U}(t)$, which can give rise to different dissipations and fluctuations through different forms of the spectral density. The solution of the Dyson equation (10) determines the evolution of the system. A general solution for such an integrodifferential equation has been derived by applying the Laplace transform. It is straightforward to apply these results to our model (5); one finds the dissipationless non-Markovian dynamics exist only when

$$G(s) = J^2 + [s + i\omega_a + f_a(s)][s + i\omega_b + f_b(s)] = 0, \tag{20}$$

where $f_m(s)$ is given by Eq. (13). This means pure imaginary roots of the above equation exist only in region $\mathrm{Im}(s) > -\omega_e$. From a physical point of view, it can also be explained by the bound state generated between the system and its environment [40,57,58]. A bound state is actually a stationary state with a vanishing decay rate during the time evolution. If such a bound state is formed, then it will lead to a dissipationless dynamics. To make this aspect clearly, we solve the eigenequation

$$\hat{H}^{\mathrm{RWA}} \left|\phi_{E_j}\right\rangle = E_j \left|\phi_{E_j}\right\rangle. \tag{21}$$

We assume one excitation is excited in the system, then

$$\left|\phi_{E_j}\right\rangle = \left[\bar{A}_a(E_j)|e,0\rangle_a + \sum_k \bar{C}_k(E_j)|g,1_k\rangle_a\right] \otimes |g,0\rangle_b + |g,0\rangle_a \otimes \left[\bar{A}_b(E_j)|e,0\rangle_b + \sum_k \bar{D}_k(E_j)|g,1_k\rangle_b\right]. \tag{22}$$

Substituting Eqs. (5) and (22) into Eq. (21), we can obtain a set of equations for $\bar{A}_a$ and $\bar{A}_b$,

$$\begin{aligned} \omega_a \bar{A}_a + J\bar{A}_b - i f_a(-iE_j)\bar{A}_a &= E_j \bar{A}_a, \\ \omega_b \bar{A}_b + J\bar{A}_a - i f_b(-iE_j)\bar{A}_b &= E_j \bar{A}_b, \end{aligned} \tag{23}$$

where $f_m(s)$ is given by Eq. (12). By solving the eigenvalue equations (23), we find the bound state exists only when

$$\det \begin{bmatrix} \omega_a - E_j - i f_a(-iE_j) & J \\ J & \omega_b - E_j - i f_b(-iE_j) \end{bmatrix} = 0, \tag{24}$$

which is equivalent to

$$K(E_j) \equiv J^2 - [\omega_a - E_j - i f_a(-iE_j)] \times [\omega_b - E_j - i f_b(-iE_j)] = 0. \quad (25)$$

Therefore, if we set $s = -iE_j$ and consider Eq. (C3), we can immediately obtain the identity

$$G(-iE_j) = K(E_j). \quad (26)$$

Therefore, we find that Eq. (20) and Eq. (25) are completely equivalent, because the zero point of denominator $G(s)$ of the Green function $\mathcal{U}(s)$ in the frequency domain reveals the eigenenergy of the whole system [43]. Based on these results, we will present an analytical treatment of eigenvalue questions in the following.

B. The purely imaginary roots for $G(s) = 0$ in region $\mathrm{Im}(s) > -\omega_e$

We now discuss the purely imaginary root for $G(s) = 0$ in Eq. (C3) in region $\mathrm{Im}(x) > -\omega_e$. If we set $s = -iE_j$ (E_j is a real number), which corresponds to identity (26), then the above equation reduces to an eigenequation (25)

$$K(E_j) = J^2 - \varphi_a(E_j)\varphi_b(E_j) = 0, \quad (27)$$

where $\varphi_m(E_j) = \omega_m - E_j - \frac{c_e}{\sqrt{\omega_e}+\sqrt{-E_j+\omega_e}}$, so $\varphi'_a(E_j) = \varphi'_b(E_j) = -1 - \frac{c_e}{2(\sqrt{\omega_e}+\sqrt{\omega_e-E_j})^2\sqrt{\omega_e-E_j}} < 0$, therefore $K'(E_j) = -\varphi'_a(E_j)[\varphi_a(E_j) + \varphi_b(E_j)]$. We can obtain extreme values E_0 by setting $K'(E_0) = 0$ being equivalent to $\varphi_a(E_0) + \varphi_b(E_0) = 0$, also $K(E_0) = J^2 + \varphi_a^2(E_0) > 0$. Therefore, we arrive at

$$\gamma(E_0) \equiv \frac{\omega_a + \omega_b}{2} - \frac{c_e}{\sqrt{\omega_e} + \sqrt{-E_0 + \omega_e}} = E_0. \quad (28)$$

The existence of a extreme value point requires that Eq. (28) has at most one real solution for $E_j < \omega_e$. It is easy to check that the solution always exists if the condition $\gamma(\omega_e) \leqslant 0$, i.e.,

$$\mu \equiv \omega_a + \omega_b - \frac{2(c_e + {\omega_e}^{3/2})}{\sqrt{\omega_e}} \leqslant 0 \quad (29)$$

is satisfied. Otherwise, no extreme value point exists, i.e., if $\mu > 0$ is satisfied. And $K(E_j)|_{E_j \to -\infty} \to -\infty$, thus there is only one real root of the equation $K(E_j) = 0$ as

$$\nu \equiv J^2 - \left(\omega_a - \omega_e - \frac{c_e}{\sqrt{\omega_e}}\right)\left(\omega_b - \omega_e - \frac{c_e}{\sqrt{\omega_e}}\right) > 0, \quad \mu \leqslant 0, \quad (30)$$

see Fig. 3(a). Based on above analysis, we summarize four regimes in Fig. 3.

Now we give the analytical expression of energy spectrum for $K(E_j) = 0$ in Eq. (27). Setting $r = E_j + \frac{c_e}{\sqrt{\omega_e}+\sqrt{-E_j+\omega_e}}$, we obtain $r_{1,2} = \frac{1}{2}[\omega_a + \omega_b \pm \sqrt{4J^2 + (\omega_a - \omega_b)^2}]$. Set $p = \sqrt{\omega_e} + \sqrt{-E_j + \omega_e}$ so the energy spectrum is

$$E_j = -p^2 + 2p\sqrt{\omega_e}, \quad (31)$$

where p satisfies cubic equation and its three roots can be obtained easily by the formula presented in the Appendix D.

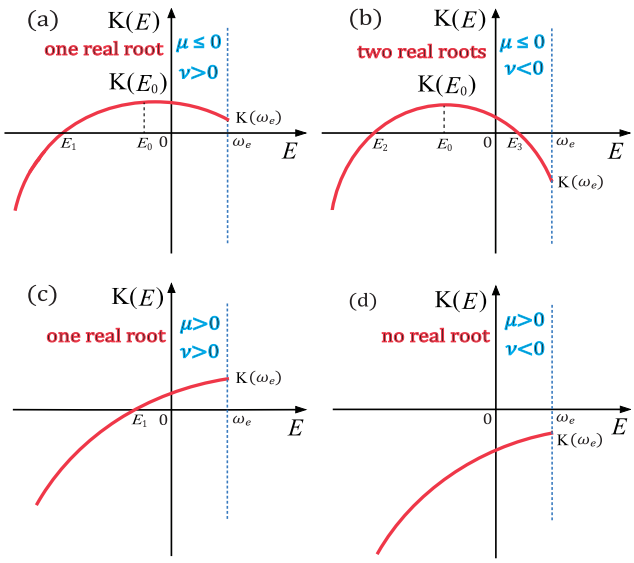

FIG. 3. Discriminants of the regions for these roots in Eq. (27).

We show that the structures of roots in $K(E_j) = 0$ in Fig. 3 play important roles in the study of non-Markovian dynamics and they completely determine the phase diagrams of the ground states of the system.

Especially, when the hopping rate J equals zero, $G_0(s)$ in Eq. (19) has at most one pure imaginary root when

$$\omega_a - \frac{c_e}{\sqrt{\omega_e}} \leqslant \omega_e, \quad (32)$$

otherwise $G_0(s)$ has no pure imaginary roots.

V. PHASE DIAGRAM

The phase diagram derived from Eqs. (29) and (30) is quite rich. Here we extend the analysis and provide more detailed discussions. For simplicity we use the following notations: phase-BS-ORR, phase with bound-state and the eigenequation (27) that has one real root (31) marked by E_1; phase-BS-TRR, phase with bound state and the eigenequation (27) that has two real roots (31) marked, respectively, by E_2 and E_3; and phase-GS-NRR, phase with ground state and the eigenequation (27) that has no real roots. Due to the hopping rate J between the two atoms, the steady-state phases can be classified into phase-BS and phase-GS. This is a general feature of the exact model and it is captured in the analytical expression by taking into account critical equation for quantum phase transitions. In the phase-GS, the population and correlation is damped, which means a vanish after long time. In the phase-BS, The population retains a finite value, which means a nonzero correlation. Yet this is not the whole story. For some values of the coupling constants, the observables can never be time independent even in the long-time limit. Instead, the system will enter an oscillatory phase in which the populations of the excited state for each atom oscillate periodically. The richness of the steady-state phase diagram arises due to all combinations that can appear. In the following we choose two different parameter spaces for phase diagram.

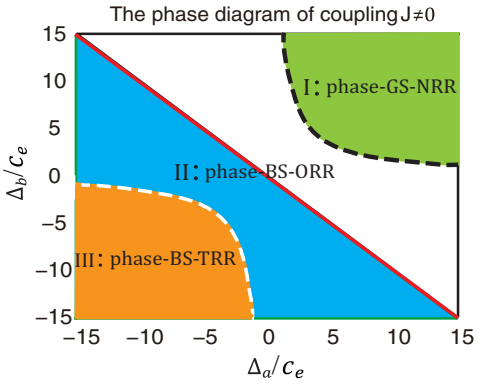

FIG. 4. (a) Phase diagram of the system for photonic crystal in the Δ_a-Δ_b plane at finite hopping J between two atoms. The white and black dashed lines denote the first critical equation in Eq. (30), while the red bold line corresponds to the critical equation (29). In this figure, the system parameters are expressed in units of c_e. We can see from the figure that the three phases cannot continuously be controlled by tuning the parameters Δ_a and Δ_b with the other fixed parameters: $\omega_e = 100c_e$, $J = 4c_e$.

A. Finite hopping rate between two atoms

Since the stationary solutions are dependent on the two detunings from the photonic band edge in photonic crystal, we plot the phase diagram in the parameter space of (Δ_a,Δ_b) in Fig. 4. Phase-BS and phase-GS governed by critical equations (29) and (30) are plotted in red bold and black and white dashed lines, respectively. Phase-GS (regime I in Fig. 4) corresponds to the decay phase. We find that the phase-BS can be detailed divided into two different phases, i.e., phase-BS-ORR (regime II in Fig. 4) and phase-BS-TRR (regime III in Fig. 4). Very clearly, the ground-state energy of the total Hamiltonian including system and environment can be shown in Fig. 5. In Fig. 5(b) with the fixed detuning $\Delta_b = -10c_e$, accompanying the formation of a bound state, the ground-state energy is changed from E_1 to E_2, which corresponds to the transition of the phase diagram from phase-BS-ORR to phase-BS-TRR, whereas with $\Delta_b = 10c_e$ in Fig. 5(c) we find the ground-state energy changes from E_g to E_1 as the detuning Δ_a crosses over its critical point, which corresponds to the change of phase from phase-GS-NRR to phase-BS-ORR. Therefore the quantum phase transition can be exactly controlled by tuning the detuning from the atom a. On the other hand, we can see from Fig. 4 that the three phases cannot continuously be controlled by tuning the parameters Δ_a and Δ_b. Instead, in the parameter space of (c_e,Δ_b) in Fig. 6, we find phases regime continuously undergo three regimes as the coupling strength c_e increases. When the detuning Δ_b is fixed, e.g., $\Delta_b = 10\omega_e$, at small c_e $(0 < c_e < 6\omega_e)$, system is in phase-GS-NRR, which corresponds to the eigenstate $|\phi_g\rangle = |g,0\rangle_a|g,0\rangle_b$ for the zero-excitation subspace. Its ground-state energy is E_g as shown in Fig. 5(a). When c_e crosses the critical point $(c_e = 6\omega_e)$, the phase-GS-NRR becomes the phase-BS-ORR, corresponding to the eigenstate $|\phi_{E_1}\rangle$ in Eq. (22) of Hamiltonian and system reaching a no inversion for steady-state population and correlation. This phase transition also corresponds to the change of ground-state energy from E_g to E_1. As c_e increases further to the value larger than $14\omega_e$,

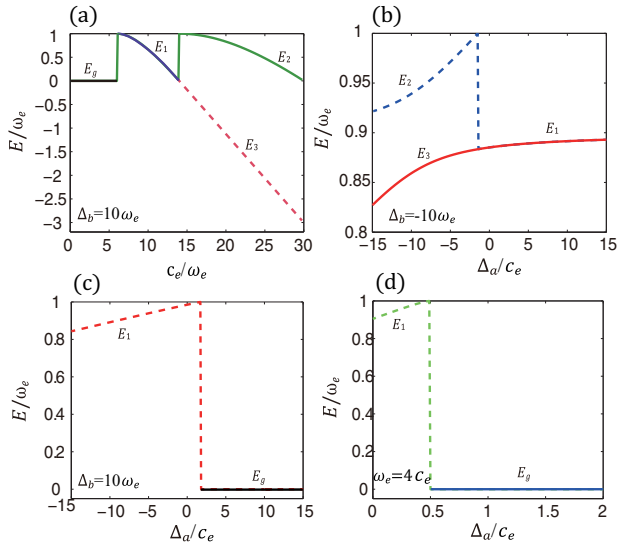

FIG. 5. Ground-state energy E of the total Hamiltonian that includes system and environment given by Eq. (31). Panel (a) corresponds to Fig. 6 with $\Delta_b = 10\omega_e$, (b) corresponds to Fig. 4 with $\Delta_b = -10\omega_e$, (c) corresponds to Fig. 4 with $\Delta_b = 10\omega_e$, while (d) corresponds to Fig. 7 with $\omega_e = 4c_e$.

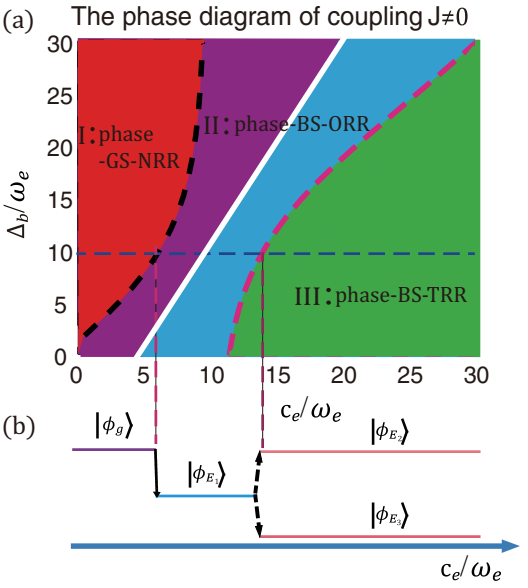

FIG. 6. (a) Phase diagram of the system for photonic crystal in the c_e-Δ_b plane at finite hopping J between two atom. The pink and black dashed lines denote the first critical equation in Eq. (30), while the white bold line corresponds to the critical equation (29). In this figure, the system parameters are expressed in units of ω_e. We can see from the figure that the three phases can continuously be controlled by tuning the parameters c_e with fixed parameters: $\Delta_a = 10\omega_e$, $J = 4\omega_e$. For example, when $\Delta_b = 10\omega_e$, the coupled strength c_e (blue dashed line) runs across this three regimes as c_e increases, which correspond to three different ground states $|\phi_g\rangle = |g,0\rangle_a|g,0\rangle_b$, $|\phi_{E_1}\rangle$, $|\phi_{E_2}\rangle$ and $|\phi_{E_3}\rangle$ in Eq. (22), respectively. Here E_j is given by Eq. (31).

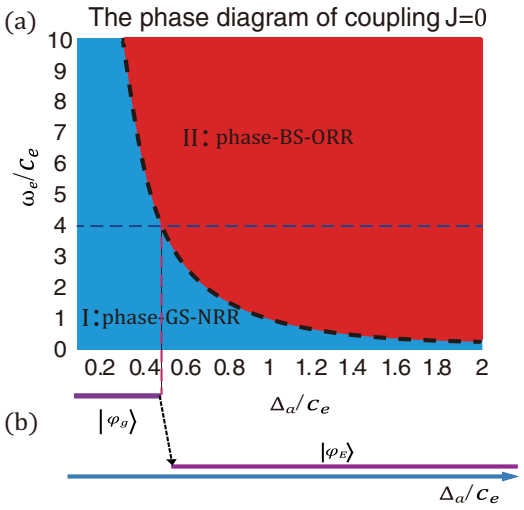

FIG. 7. (a) Phase diagram of the system for photonic crystal in the Δ_a-ω_e plane at zero hopping. The black-dashed lines denote the critical equation (32). We find that there is no phase-BS-TRR when the hopping rate $J = 0$.

the phase-BS-ORR becomes phase-BS-TRR, corresponding to the two eigenstates $|\phi_{E_2}\rangle$ and $|\phi_{E_3}\rangle$ in Eq. (22) of the Hamiltonian and giving rise to a pair of real roots given by Eq. (31) and the system enters the oscillatory phase. In the aspect of ground-state energy, this quantum transition can be shown in Fig. 5(a) with the transition of the ground-state energy from E_1 to E_2.

B. Zero hopping rate between two atoms

For the situation in which the two atoms decouples each other, the phase structure can be divided into two phases. In Fig. 7, when ω_e is fixed, at small Δ_a there exists only the phase-GS-NRR, and as Δ_a crosses the critical point ($\Delta_a = 0.5c_e$), the system enters the phase-BS-ORR. From the aspect of the ground-state energy in Fig. 5(d), the quantum phase transition can be further verified by the change of the ground-state energy from E_g to E_1. We find the phase-BS-TRR does not exist in this case due to the vanishing hopping rate. The result with a bound state is consistent with earlier works [34–36].

VI. TIME EVOLUTION AND LONG-TIME BEHAVIOR FOR POPULATION AND CORRELATION

Equations (15) and (16) provide general solutions of the non-Markovian dissipative dynamics for the system of two coupled atoms in three-dimensional photonic crystal structures. It shows that the atoms dynamics in photonic crystal always contains two parts: a localized photon mode (the first term) and nonlocalized mode (the other terms except the first term) photon damping. The localized mode is a long-lived non-Markovian effect (dissipationless), induced by the PBG structure in photonic crystal. The corresponding frequency-energy spectrum always exists within the PBG. This nonlocalized mode damping is a short-time non-Markovian memory effect, and it will become an exponential (Markovian) decay in the photonic band (PB) region, as we will show later. The contributions of both the localized and the nonlocalized mode damping strongly rely on the detunings Δ_a and Δ_b.

In Fig. 2(b), we plot the localized exciton mode eigenspectras E_j given by Eq. (31) as a function of the detuning. In this case, the values of the localized mode eigenspectras correspond to three different detunings from the edge of photonic band of photonic crystal. The importance of the localized photon mode is determined by the localized exciton mode amplitude, $\sum_j \frac{m(-iE_j)}{G'(-iE_j)}$ ($m = m_1, m_3$) given in Eqs. (17) and (18), which is plotted in Fig. 2(d) as a function of the detuning Δ_a for three different detunings Δ_b. The results presented in Figs. 2(b) and 2(d) provide indeed the full steady-state information of the exciton dynamics. This is because the nonlocalized mode photon damping [i.e., the second and third terms in Eqs. (15) and (16)] will decay to zero so only the localized photon mode contributes to the steady-state exciton probability amplitudes. In other words, the steady state exciton amplitude quantifies the contribution of the localized photon mode as a dissipationless effect.

With the help of the probability amplitudes in Eq. (A2) with Eqs. (15) and (16), we can now express the reduced density matrix $\rho(t)$ of the two-qubit as

$$\rho(t) = \mathrm{Tr}_{R_a+R_b}|\psi(t)\rangle\langle\psi(t)| = \begin{pmatrix} 0 & 0 & 0 & 0 \\ 0 & |A_a(t)|^2 & A_a^*(t)A_b(t) & 0 \\ 0 & A_a(t)A_b^*(t) & |A_b(t)|^2 & 0 \\ 0 & 0 & 0 & A(t) \end{pmatrix}, \quad (33)$$

where $A(t) = 1 - |A_a(t)|^2 - |A_b(t)|^2$ and $\mathrm{Tr}_{R_a+R_b}$ denote a trace over the two environments.

We now investigate the time evolution of quantum correlations of a two-qubit state. For X states described by Eq. (33), the concurrence [59,60] and discord [61] can be described by [62,63]

$$C = 2|A_a(t)A_b(t)|, \qquad D = \min\{Q_1, Q_2\}, \quad (34)$$

where $Q_j = h(\rho_{11}+\rho_{33}) + \sum_{k=1}^4 \lambda_k \log_2 \lambda_k + \mu_j, h(x) = -x\log_2 x - (1-x)\log_2(1-x)$ is the binary entropy. Here $\mu_1 = h(\tau)$, where $\tau = \frac{1}{2}\{1 + \sqrt{[1-2(\rho_{33}+\rho_{44})]^2 + 4(|\rho_{14}|+|\rho_{23}|)^2}\}$ and $\mu_2 = -\sum_{k=1}^4 \rho_{kk}\log_2\rho_{kk} - h(\rho_{11}+\rho_{33})$.

(I) *Complete decay of population and correlation (phase-GS-NRR).* We discuss in detail the features of three different phases in Fig. 4, since the range of the phases is given exactly by Eqs. (29) and (30). First, in the PB region (phase-GS-NRR in Fig. 4), where the localized mode vanishes due to there being no real root in PB, the exciton dynamics undergoes a full dissipation process, see Fig. 8, and can be approximately characterized as a nonlocalized mode, which contains two parts: One is the second term in Eqs. (15) and (16), which is the oscillating damping process due to the complex roots in $L(s) = 0$ in the regime of [$\mathrm{Re}(s) < 0$ and $\mathrm{Im}(s) < -\omega_e$]. The other is the integral part, i.e., the nonexponential parts will oscillate rapidly in time. This rapidly oscillating damping originates from the terms containing $e^{i\omega_e t}$ in Eq. (16). This has no physical consequence because the photon dissipation

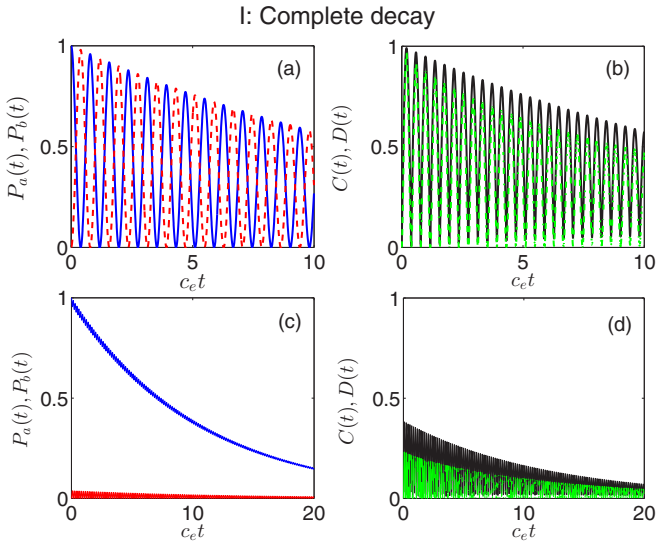

FIG. 8. The time evolution of the population and quantum correlation. The blue dashed and red solid lines denote the population $P_a(t) = |A_m(t)|^2$ for atom a and atom b, respectively. The black dashed and green solid lines correspond to concurrence and quantum discord, respectively. The initial state takes $A_a(0) = 1, A_b(0) = 0$. This case corresponds to the phase-GS-NRR for the regime I in Fig. 4. The parameters chosen are $\omega_e = 100c_e$, $\Delta_b = 10c_e$, and $J = 4c_e$, $\Delta_a = 10c_e$ for (a) and (b) and $\Delta_a = 50c_e$ for (c) and (d).

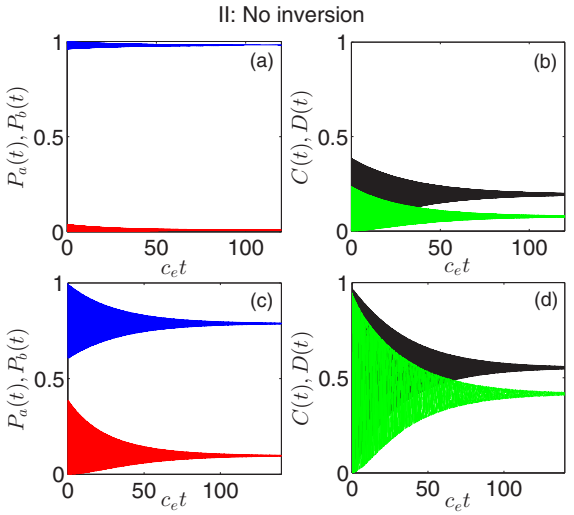

FIG. 9. Same as Fig. 8. In this case, the atom frequency tuned into the phase-BS-ORR for the regime II in Fig. 4. The parameters chosen are $\omega_e = 100c_e$, $J = 4c_e$. $\Delta_a = -30c_e$ for (a) and (b) and $\Delta_a = 0$ for (b) and (d).

is almost completed after this point of time. In addition, we can find that the monotonicity of the quantum discord and concurrence is similar on the whole, and the former is larger than the latter. They always rapidly approach to zero after a long time.

(II) *No population inversion of population and correlation* (*phase-BS-ORR*). The nonlocalized mode parts will rapidly approach zero within the PBG (phase-GS-NRR in Fig. 4) according to the Lebesgue-Riemann lemma. In phase-BS-ORR, there is only one real energy spectrum, therefore the population (17) and (18) and correlations can be obtained (see Fig. 9) after a long time,

$$\begin{aligned} P_a(\infty) &= \frac{m_1(-iE_1)}{G'(-iE_1)}, \\ P_b(\infty) &= \frac{m_3(-iE_1)}{G'(-iE_1)}, \\ C(\infty) &= 2\frac{m_1(-iE_1)}{G'(-iE_1)}\frac{m_3(-iE_1)}{G'(-iE_1)}, \end{aligned} \tag{35}$$

where quantum discord is too cumbersome and is not presented here. E_1 is a real root in Eq. (31). We find that population and correlation hold a nonzero steady value after a long time. This is also understandable based on the fact that the bound state, as a stationary state of the whole system, has a vanishing decay rate and the coherence contained in it would be preserved during the time evolution.

(III) *Periodic oscillation of population and correlation* (*phase-BS-TRR*). Interestingly, in regime of phase-BS-TRR, the quantum interference effects between the two localized modes after large time t lead to periodic oscillation behaviors of the dynamics. The amplitudes of periodic oscillations do not decrease in time. From Eqs. (17) and (18), we obtain the populations in the long-time regime:

$$\begin{aligned} P_a(t \to \infty) &= \varepsilon_1^2\varepsilon_2^2 + \varepsilon_1\varepsilon_2\cos[(E_2 - E_3)t], \\ P_b(t \to \infty) &= \varepsilon_3^2\varepsilon_4^2 + \varepsilon_3\varepsilon_4\cos[(E_2 - E_3)t], \end{aligned} \tag{36}$$

whose periodic is $T = 2\pi/(E_2 - E_3)$. Here E_j $(j = 2,3)$ is the real root in Eq. (31), these coefficients take $\varepsilon_1 = \frac{m_1(-iE_2)}{G'(-iE_2)}, \varepsilon_2 = \frac{m_1(-iE_3)}{G'(-iE_3)}, \varepsilon_3 = \frac{m_3(-iE_2)}{G'(-iE_2)}, \varepsilon_4 = \frac{m_3(-iE_3)}{G'(-iE_3)}$. The dynamics reaches periodic oscillation behaviors. In other words, the nonlocalized mode will approach zero after some time due to the localized exciton dynamics. The short-time dynamics is given by Fig. 10, which falls into the regime of phase-BS-TRR in Fig. 4. For long-time dynamics behavior, we present the variations of population and correlations given by Eqs. (34) and (36) in Fig. 11. In Figs. 11(a) and 11(b), we find that phase transition only occurs between phase-BS-ORR and phase-BS-TRR with fixed Δ_a, which corresponds to the phase diagram in Fig. 4. However, in Figs. 11(c) and 11(d), we find there are three phases continuously over through the phase transition point, i.e., concurrence and discord vary from zero to a time-independent steady value and, further, to periodic oscillation, which corresponds to regimes I, II, and III of the phase diagram in Fig. 6, respectively.

VII. GROUND-STATE FIDELITY AND ENTANGLEMENT ENTROPY

With the help of ground-state fidelity and entanglement entropy, we can further confirm that a quantum phase transition exists in the system of atoms and the photonic crystals. The ground-state fidelity is defined as the overlap of two ground states corresponding to two slightly different control parameters $F = \langle\phi_{E_j}(\Delta_b)|\phi_{E_j}(\Delta_b + \delta\Delta_b)\rangle$ [64]. The entanglement entropy $\varepsilon = -\rho\log_2\rho = -\sum_k \lambda_k\log_2\lambda_k$ [65,66] can be obtained by calculating the entropy of the reduced density matrix (33) of the two atoms after tracing out the reservoir's

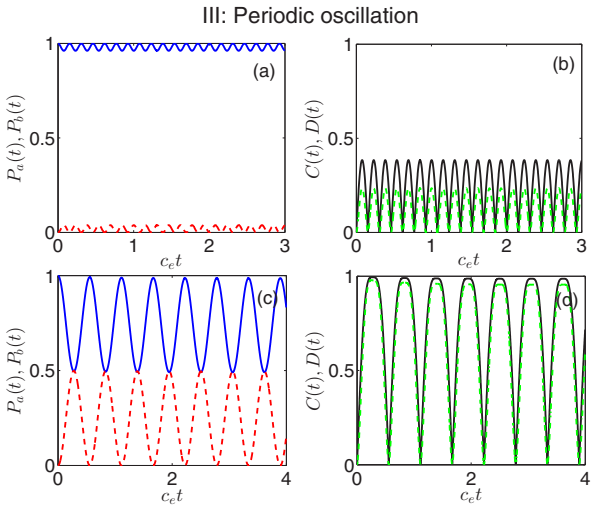

FIG. 10. Same as Fig. 8. In this case, the atom frequency tuned into the phase-BS-TRR for the regime III in Fig. 4. The two localized modes reach steady values with the time oscillation, whose period is $T = 2\pi/|E_2 - E_3|$, where E_2 and E_3 are the two real roots in Eq. (31). The parameters chosen are $\omega_e = 100c_e$, $J = 4c_e$. $\Delta_b = -10c_e$, $\Delta_a = -50c_e$ for (a) and (b) and $\Delta_a = -2c_e$ for (b) and (d).

degrees of freedom. In order to further verify the existence of the quantum phase transition in this system, we plot F near the critical points in Figs. 12(a) and 12(b). The singularity in the plot clearly shows the existence of quantum phase transition in this model. Because of the totally orthogonal property of the ground state, the fidelity completely drops to zero at the critical point. In Figs. 12(c) and 12(d), we plot ε of the ground state, which only corresponds to the eigenspectra E_2 in Eq. (31). This shows the phase transitions between phase-GS-NRR and phase-BS-ORR. Near the critical point, we find a sudden birth

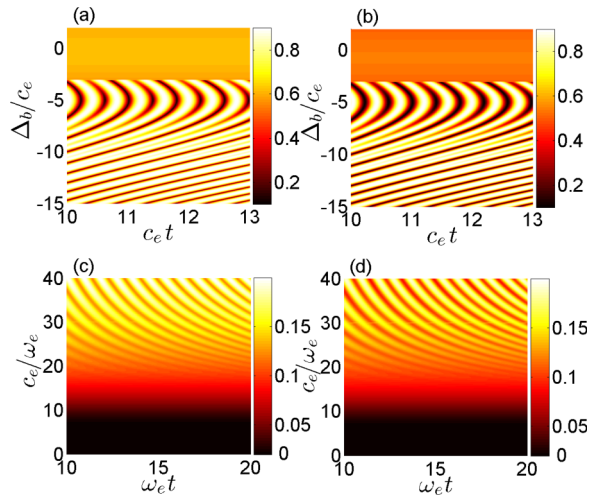

FIG. 11. The long-time concurrence [(a) and (c)] and discord [(b) and (d)] as a function of different parameters. Parameters chosen are $\omega_e = 100c_e$, $\Delta_a = -5c_e$, $J = 4c_e$ for (a) and (b) and $\Delta_a = \Delta_b = 10\omega_e$, $J = 4\omega_e$, for (c) and (d). Panels (a) and (b) correspond to the regime II, and III in Fig. 4, while panels (c) and (d) fall into the regimes I, II, and III in Fig. 6.

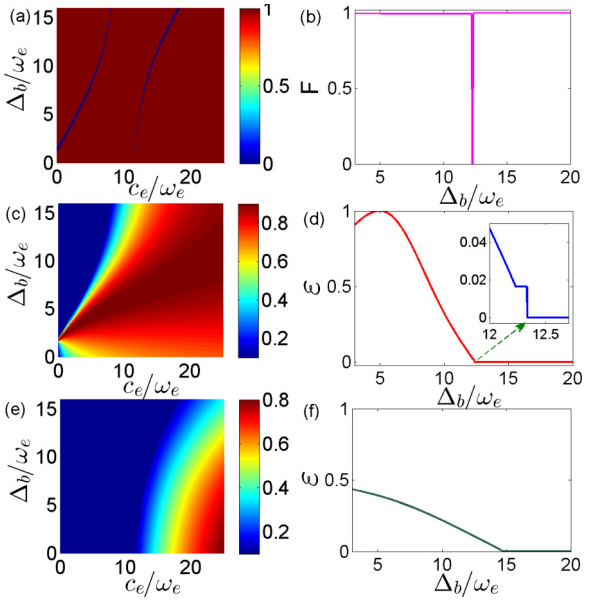

FIG. 12. Ground-state fidelity in (a) and (b) and entanglement entropy in (c), (d), (e), and (f) as functions of the coupling and detuning. Parameters chosen are $\Delta_a = 10\omega_e$, $J = 4\omega_e$ for (a), (c), and (e); $c_e = 7\omega_e$ for (b) and (d); and $c_e = 17\omega_e$ for (f). Here (c) and (d) only correspond to the eigenspectra E_2 in Eq. (31), while (e) and (f) only correspond to the eigenspectra E_3. This case falls into regimes I, II, and III in Fig 6.

of the ground-state entanglement, which can be seen as a result of the changing ground-state structure. This discontinuity in the ground-state entanglement entropy also evidently shows the existence of the quantum phase transition. Furthermore, Figs. 12(e) and 12(f) are plotted by eigenspectra E_3, which corresponds to the phase transitions between phase-BS-ORR and phase-BS-TRR. This case corresponds to the phase diagram in Fig. 6. This dynamical behavior in turn confirms the existence of the bound-state-induced QPT in the system. The sudden transition from complete decoherence to decoherence suppression and then to periodic oscillation results from the occurrence of QPT in the model itself. It is the abrupt change of the ground-state structure near the critical point of the QPT that induces the qualitative difference in the system dynamics.

VIII. THE QUANTUM PHASE TRANSITION WITHOUT THE RWA

In this section, we study influence of the nonrotating wave terms on the QPT in the coupled spin-boson models. We first recover the delocalized-localized QPT. Then, using the perturbation approach based on unitary transform [22–24], we study the properties of the ground state for the total system in the delocalized regime.

In order to take into account the correlation between spin and bosons, we present a treatment based on the unitary transform to $\hat{H}' = e^S \hat{H} e^{-S}$, where the generator of the transform is $S = \sum_{m,k} \frac{V_{m,k}\xi_{k,m}}{2\omega_m}(\hat{b}^\dagger_{m,k} - \hat{b}_{m,k})\sigma^x_m$. A k-dependent function $\xi_{k,m}$ introduced in the transform corresponds to the displacement of each boson mode due to the coupling to the two-state system [23,24,67]. Its form will be determined later

by the perturbation theory. The transform can be done and the result is $\hat{H}' = \sum_{m=a,b} \hat{H}'_{0,m} + \hat{H}'_{1,m} + \hat{H}_{ab}$ with

$$\hat{H}'_{0,m} = \eta_m \omega_m \sigma_m^+ \sigma_m^- + \sum_k \hbar\omega_{m,k} \hat{b}^\dagger_{m,k} \hat{b}_{m,k} + C_m,$$

$$\hat{H}'_{1,m} = \sum_k \frac{V_{m,k}(1-\xi_{k,m})}{2} (\hat{b}^\dagger_{m,k} + \hat{b}_{m,k}) \sigma_m^x - i\frac{\omega_m}{2}\sigma_m^y \sinh\hat{\varphi}_m + \frac{\omega_m}{2}\sigma_m^z(\cosh\hat{\varphi}_m - \eta_m), \tag{37}$$

where $C_m = \sum_k \frac{V_{m,k}^2}{4\omega_m}\xi_{k,m}(\xi_{k,m}-2)$, $\hat{\varphi}_m = \sum_k \frac{V_{m,k}\xi_{k,m}}{\omega_{m,k}}(\hat{b}^\dagger_{m,k} - \hat{b}_{m,k})$, and defined renormalized factor

$$\eta_m = \langle\{0_k\}|\cosh\hat{\varphi}_m|\{0_k\}\rangle = \exp\left[-\sum_k \frac{V_{m,k}^2\xi_{k,m}^2}{2\omega_m^2}\right]. \tag{38}$$

Following the variational method [22,23,26], the transformed parameters

$$\xi_{k,m} = \frac{\omega_{m,k}}{\omega_{m,k} + \eta_m\omega_m}, \tag{39}$$

can be determined by minimizing the Bogoliubov-Peierls free energy. The renormalized factor η_m in Eq. (38) has been used successfully to characterize the delocalized-localized QPT [22,23]. If the tunneling amplitude is renormalized to zero, then the system is in the localized phase and the dynamics is trivial. In contrast, if the renormalized tunneling amplitude is nonzero, then the system is in the delocalized phase, which displays some interesting dynamical behaviors such as damped coherent oscillation and incoherent relaxation [14]. Solving Eqs. (38) and (39) with Eqs. (3) and (4), we obtain transcendental equation to renormalized factor η_m,

$$\eta_m = \exp\left\{-\frac{c_e[2\omega_e + \omega_m\eta_m - 2\sqrt{\omega_e(\omega_e+\omega_m\eta_m)}]}{4\omega_m^2\eta_m^2\sqrt{\omega_e+\omega_m\eta_m}}\right\}. \tag{40}$$

In Fig. 13, we plot the numerical results on this QPT characterized by the renormalized factor η, which can be calculated by Eq. (40), where $\eta_a = \eta_b \equiv \eta$ has been assumed

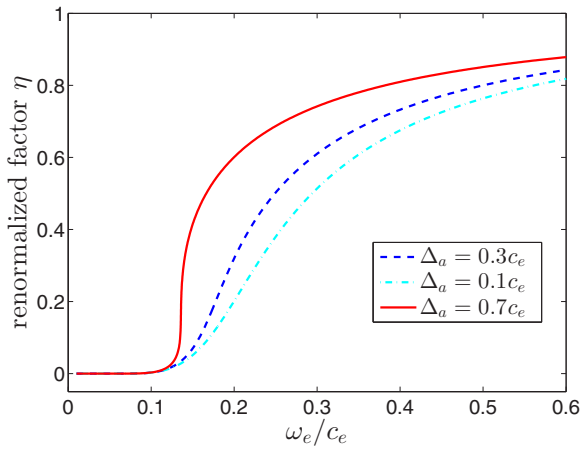

FIG. 13. The delocalized-localized QPT characterized by the renormalized factor η as a function of the the band edge of the photonic crystal ω_e.

due to $\omega_a = \omega_b$. We can see that the system is in the delocalized phase regime when ω_e is large, where η takes a finite value. With the decrease of ω_e, η drops suddenly to zero and the system enters the localized phase regime, which is coincident with the results under the quantum Monte Carlo method and the numerical diagonalization method [12,26].

Focusing on the delocalized phase regime, which occurs in the weak-coupling limit, we further separate the first-order perturbation term from $\hat{H}'_{1,m} = \sum_{m=a,b} \hat{H}'_{2,m} + \hat{H}'_{3,m}$ with

$$\hat{H}'_{2,m} = \sum_k \lambda_{m,k}(\hat{b}_{m,k}\sigma_m^+ + \text{H.c.}),$$

$$\hat{H}'_{3,m} = \frac{\omega_m}{2}\sigma_m^z(\cosh\hat{\varphi}_m - \eta_m) - i\frac{\omega_m}{2}\sigma_m^y(\sinh\hat{\varphi}_m - \eta_m\hat{\varphi}_m), \tag{41}$$

where $\lambda_{m,k} = \eta_m\omega_m V_{m,k}\xi_{k,m}/\omega_{m,k}$. Combining with Eq. (37), we transformed our model as $\hat{H}' = \sum_{m=a,b}\hat{H}'_{0,m} + \hat{H}'_{2,m} + \hat{H}'_{3,m}$, where $\hat{H}'_{0,m}$ collects all the renormalized noninteracting terms, $\hat{H}'_{2,m}$ collects all the first-order perturbation terms, and $\hat{H}'_{3,m}$ collects all the higher-order ones. It has been proved that in zero-temperature and weak-coupling regimes, the higher-order perturbation terms $\hat{H}'_{3,m}$ can be neglected [23,24] due to the fact $\langle\phi_r|\hat{H}'_{3,m}|\phi_r\rangle = 0, r = g, E_1, E_2$, and E_3 in zero and single-exciton eigenspaces. Thus the Hamiltonian takes the form of $\hat{H}' \approx \sum_{m=a,b}\hat{H}'_{0,m} + \hat{H}'_{2,m} \equiv \hat{H}_{\text{eff}}$,

$$\hat{H}_{\text{eff}} = \hat{H}_a^{\text{NRWA}} + \hat{H}_b^{\text{NRWA}} + \hat{H}_{ab}^{\text{RWA}}, \tag{42}$$

with

$$\hat{H}_m^{\text{NRWA}} = \hbar\eta_m\omega_m\sigma_m^+\sigma_m^- + \sum_k[\hbar\lambda_{m,k}\hat{b}_{m,k}\sigma_m^+ + \text{H.c.}] + \sum_k \hbar\omega_{m,k}\hat{b}^\dagger_{m,k}\hat{b}_{m,k} + C_m,$$

$$\hat{H}_{ab}^{\text{RWA}} = \hbar J\sigma_a^+\sigma_b^- + \hbar J\sigma_a^-\sigma_b^+, \tag{43}$$

which is similar to the RWA Hamiltonian (5) except the renormalized factor η_m and the coupling strength $\lambda_{m,k}$. By means of the similar method with Sec. IIB, we plot the energy spectrum in Fig. 14. In the delocalized phase regime we worked, where η_m takes a finite value, we now verify the QPT by studying the ground-state energy of the total system including the environments in Fig. 14. We find that the ground-state energy E is discontinuous at the critical point where the bound state is formed. It manifests clearly that there is a QPT existing in the delocalized phase regime.

The system described by the coupled spin-boson models under a perturbation approach in the delocalized phase occurring in the weak-coupling limit at zero temperature has been investigated analytically. We can see that the QPT induced by the formation of the bound state has a profound impact on the system dynamics of the TLS in the delocalized phase regime. It induces a dynamical transition from complete decoherence to decoherence suppression with only the single-excitation subspace.

We now discuss the realizability of our model in realistic materials. A N-period one dimensional lattice reproduces a band gap via appropriate sequences of dielectric unit cells and an arbitrarily shaped density of frequency modes can be

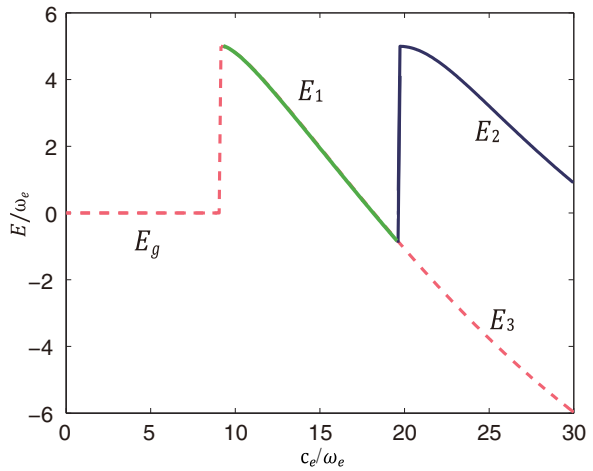

FIG. 14. Ground-state energy E of the total Hamiltonian including system and environment given by Eq. (31). (a) Corresponding to Fig. 6 with $\Delta_b = 10\omega_e$ in delocalized regime $\eta_a = \eta_b \equiv \eta \neq 0$.

modeled through the sequence of the transmission coefficients of each unit cell [68]. The corresponding environment may be realized via diffractive grating and photonic crystals engineered 1D PBG microcavities [69,70]. Therefore, the present theoretical approach provides a way to model the environment light-matter systems, suitable to protect coherence [71–73]. As a result, the present analytical result has a highly advantageous means of maintaining high fidelity of quantum states and quantum-logic operations in the presence of decay and decoherence in the realistic materials.

IX. DISCUSSION

In this paper, QPTs through two two-level atoms embedded in a three-dimensional anisotropic photonic crystal have been investigated both with and without RWA. When the RWA is applied to this model in weak-coupling limit, we derive the exact time evolution dynamics of the system by Laplace transform. By applying Green function approach to the ground state of the whole Hamiltonian, we obtain the phase diagram by analytically giving two exact critical equations. Two QPTs occur in our system, and different ground states are associated with three phases with two critical equations, which correspond to zero-exciton eigenstate, single-exciton eigenstate with a real eigenvalue, and single-exciton eigenstates with two real eigenvalues, which we label (I)–(III), respectively. The first QPT occurs between phases I and II, where the first QPT, i.e., from phase I to phase II, occurs when we control the detuning over the critical points. The existence of the second QPT originated from the transition of two bound states in single-exciton subspace. This novel bound state shows the period oscillation behavior for the system, which arises from the quantum interference of two localized modes.

When the RWA breaks down, making use of the perturbation approach to neglect the high-order interaction terms in a unitarily transformed Hamiltonian, we have shown that the QPT still exists in the delocalized phase regime. The approximation is valid in the weak-coupling regime under zero temperature, where the high-order excitations are negligible. We also further confirmed that the neglected terms give no contribution to the QPT, which validates our approximations. Our purely analytical treatment provides a unified microscopic description of the QPTs and renders a helpful understanding of the rich physics in the TLS. This simple proposal provides an effective means that has potential application in quantum devices and quantum statistics.

ACKNOWLEDGMENTS

We thank Dr. Q. J. Tong and Dr. S. L. Su for valuable discussions. This work is supported by the National Natural Science Foundation of China (Grants No. 11175032, No. 61475033, No. 11204028, and No. 11405026) and the Fundamental Research Funds for the Central Universities (Grant No. 14QNJJ008).

APPENDIX A: THE DERIVATION OF THE DYSON EQUATION (13)

It is easy to verify that the exciton number operator

$$\hat{N} = \sum_{m=a,b} \sigma_m^+ \sigma_m^- + \hat{b}_{m,k}^\dagger \hat{b}_{m,k} \tag{A1}$$

is a conserved quantity due to the fact that commutation relation $[\hat{H}^{\mathrm{RWA}}, \hat{N}] = 0$. Taking the initial state (7), the time-evolved state $|\psi(t)\rangle$ can be written as

$$\begin{aligned} |\psi(t)\rangle = & \left[A_a(t)|e,0\rangle_a + \sum_k C_k(t)|g,1_k\rangle_a \right] \otimes |g,0\rangle_b \\ & + |g,0\rangle_a \otimes \left[A_b(t)|e,0\rangle_b + \sum_k D_k(t)|g,1_k\rangle_b \right] \\ & + A_0|g,0\rangle_a|g,0\rangle_b, \end{aligned} \tag{A2}$$

in which the amplitude A_0 is constant since $\hat{H}^{\mathrm{RWA}}|g,0\rangle_a|g,0\rangle_b = 0$, while A_m, C_k, and D_k are time-dependent quantities, where $|0\rangle_m = \prod_k |0_k\rangle_m$, $|1_k\rangle = |0_0\rangle \otimes \cdots |0_{k-1}\rangle \otimes |1_k\rangle \otimes |0_{k+1}\rangle \cdots$. By substituting $|\psi(t)\rangle$ into the Schrödinger equation $i\frac{\partial}{\partial t}|\psi(t)\rangle = \hat{H}^{\mathrm{RWA}}|\psi(t)\rangle$ (hereafter, $\hbar = 1$), we obtain

$$\begin{aligned} \frac{dA_a(t)}{dt} &= -i\omega_a A_a(t) - iJA_b(t) - i\sum_k V_{a,k}C_k(t), \\ \frac{dA_b(t)}{dt} &= -i\omega_b A_b(t) - iJA_a(t) - i\sum_k V_{b,k}D_k(t), \\ \frac{dC_k(t)}{dt} &= -iA_a(t)V_{a,k}^* - i\omega_{a,k}C_k(t), \\ \frac{dD_k(t)}{dt} &= -iA_b(t)V_{b,k}^* - i\omega_{b,k}D_k(t). \end{aligned} \tag{A3}$$

By formally integrating the last two equations in Eq. (A3) and substituting the result into the first two equations in Eq. (A3),

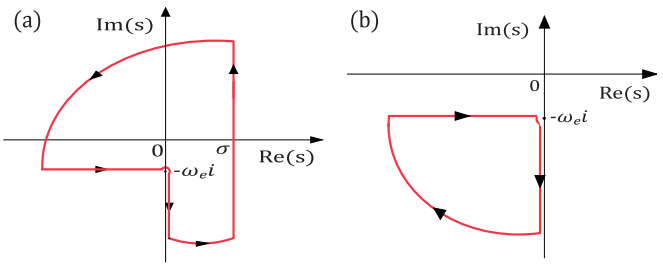

FIG. 15. The integration contours for Eq. (C2).

we arrive at

$$\dot{A}_a(t) = -i\omega_a A_a(t) - iJA_b(t) - \int_0^t A_a(\tau) f_a(t-\tau)d\tau,$$
$$\dot{A}_b(t) = -i\omega_b A_b(t) - iJA_a(t) - \int_0^t A_b(\tau) f_b(t-\tau)d\tau, \tag{A4}$$

where the fluctuation dissipation relation

$$f_m(t) = \sum_k |V_{m,k}|^2 e^{-i\omega_{m,k}t}. \tag{A5}$$

Therefore Eq. (10) can be obtained by substituting Eq. (A4) into Eq. (9).

APPENDIX B: THE CALCULATION OF $f_m(s)$

With Eq. (3), we can calculate $f_m(s)$ in Eq. (11) as follows:

$$\begin{aligned} f_m(s) &= \sum_m \frac{|V_{m,k}|^2}{s+i\omega_{m,k}} \\ &= \frac{(\omega_m d_m)^2}{2\varepsilon_0\hbar V}\sum_k \frac{(\vec{e}_k\cdot\vec{u}_d)(\vec{e}_k\cdot\vec{u}_d)}{\omega_{m,k}[s+i\omega_{m,k}]} \\ &= \frac{(\omega_m d_m)^2}{2\varepsilon_0\hbar V}\sum_k \frac{1-(\vec{k}\cdot\vec{u}_d)^2/k^2}{\omega_{m,k}[s+i\omega_{m,k}]} \\ &= \frac{(\omega_m d_m)^2}{16\pi^3\varepsilon_0\hbar}\int \frac{[1-(\vec{k}\cdot\vec{u}_d)^2/k^2]d^3\vec{k}}{\omega_{m,k}[s+i\omega_{m,k}]}, \end{aligned} \tag{B1}$$

where we have replaced the sum by an integral via $\sum_k \to \frac{V}{(2\pi)^3}\int d^3\vec{k}$ and $(\vec{e}_k\cdot\vec{u}_d)(\vec{e}_k\cdot\vec{u}_d) = 1-(\vec{k}\cdot\vec{u}_d)(\vec{k}\cdot\vec{u}_d)/k^2$. Near the band edge, the dispersion relation may be expressed approximately by $\omega_{m,k} = \omega_e + B_m|\vec{k}-\vec{k}_0^j|^2$. The angle between the dipole vector of the atom and the j-th $\vec{k}_0^j$ is θ_j. The angle between the dipole and $\vec{k}$ near $\vec{k}_0^j$ is replaced approximately by θ_j. We calculate $f_{m,k}$ as follows:

$$\begin{aligned} f_m(s) &= \frac{(\omega_m d_m)^2}{16\pi^3\varepsilon_0\hbar}\int \frac{[1-(\vec{k}\cdot\vec{u}_d)^2/k^2]d^3\vec{k}}{\omega_{m,k}[s+i\omega_{m,k}]} \\ &= \frac{(\omega_m d_m)^2}{16\pi^3\varepsilon_0\hbar}\left(\sum_{j_1}\sin^2\theta_{j_1}\right)\int \frac{d^3\vec{q}}{(\omega_e+B_m|\vec{q}|^2)[s+i(\omega_e+B_m|\vec{q}|^2)]} \\ &= \frac{(\omega_m d_m)^2}{4\pi^2\varepsilon_0\hbar}\left(\sum_{j_1}\sin^2\theta_{j_1}\right)\int_0^\infty \frac{q^2dq}{(\omega_e+B_m q^2)[s+i(\omega_e+B_m q^2)]}. \end{aligned} \tag{B2}$$

Consequently, integrating the last line in above equation, we obtain Eq. (13).

APPENDIX C: THE CALCULATION OF THE AMPLITUDES $A_a(t)$ AND $A_b(t)$

The amplitude $A_a(t)$ can be obtained by means of the inverse Laplace transform [51–54],

$$A_a(t) = \frac{1}{2\pi i}\int_{\sigma-i\infty}^{\sigma+i\infty} A_a(s)e^{st}ds = \frac{1}{2\pi i}\int_{\sigma-i\infty}^{\sigma+i\infty} dse^{st}\frac{-iA_b(0)J + A_a(0)\left[s+i\omega_b - \frac{ic_m}{\sqrt{\omega_e}+\sqrt{-is+\omega_e}}\right]}{J^2+\left[s+i\omega_a-\frac{ic_m}{\sqrt{\omega_e}+\sqrt{-is+\omega_e}}\right]\left[s+i\omega_b-\frac{ic_m}{\sqrt{\omega_e}+\sqrt{-is+\omega_e}}\right]}. \tag{C1}$$

With the integration contours as shown in Fig. 15(a), we have

$$A_a(t) = \sum_j \frac{m_1(x_j^{(1)})e^{x_j^{(1)}t}}{G'(x_j^{(1)})} - \frac{1}{2\pi i}\left[\int_{-i\omega_e-\infty}^{-i\omega_e+0} + \int_{-i\omega_e+0}^{-i\infty+0} dse^{st}\frac{-iA_b(0)J + A_a(0)\left[s+i\omega_b-\frac{ic_m}{\sqrt{-is+\omega_e}}\right]}{J^2+\left[s+i\omega_a-\frac{ic_m}{\sqrt{-is+\omega_e}}\right]\left[s+i\omega_b-\frac{ic_m}{\sqrt{-is+\omega_e}}\right]}\right], \tag{C2}$$

where the function

$$\begin{aligned} m_1(s) &= -iA_b(0)J + A_a(0)[s+i\omega_b+\alpha(s)], \\ G(s) &= J^2 + [s+i\omega_a+\alpha(s)][s+i\omega_b+\alpha(s)], \end{aligned} \tag{C3}$$

where $\alpha(s) = -\frac{ic_m}{\sqrt{\omega_e}+\sqrt{-ix+\omega_e}}$, and $x_k^{(1)}$ is the root of the equation $G(s)=0$ in the region [Re$(s)>0$ or Im$(s)>-\omega_e$], the real number σ, and the real number $s=\sigma$ lies to the right of all the singularities $x_j^{(1)}$. The last term can be calculated with the

integration contours as shown in Fig. 15(b):

$$\begin{aligned}
&\frac{1}{2\pi i}\int_{-i\omega_e+0}^{-i\infty+0} ds e^{st}\frac{-iA_b(0)J+A_a(0)[s+i\omega_b+\alpha(s)]}{J^2+[s+i\omega_a+\alpha(s)][s+i\omega_b+\alpha(s)]}\\
&=\frac{1}{2\pi i}\int_{-i\omega_e}^{-i\infty} ds e^{st}\frac{-iA_b(0)J+A_a(0)[s+i\omega_b+\beta(s)]}{J^2+[s+i\omega_a+\beta(s)][s+i\omega_b+\beta(s)]}\\
&=-\sum_j \frac{m_2\left(x_j^{(2)}\right)e^{x_j^{(2)}t}}{L'\left(x_j^{(2)}\right)}-\frac{1}{2\pi i}\left[\int_{-i\omega_e-\infty}^{-i\omega_e+0} ds e^{st}\frac{-iA_b(0)J+A_a(0)[s+i\omega_b+\beta(s)]}{J^2+[s+i\omega_a+\beta(s)][s+i\omega_b\beta(s)]}\right],
\end{aligned} \tag{C4}$$

where

$$L(s)=J^2+[s+i\omega_a+\beta(s)][s+i\omega_b+\beta(s)], \tag{C5}$$

where $\beta(s)=-\frac{ic_m}{\sqrt{\omega_e}-i\sqrt{is-\omega_e}}$, and $x_k^{(2)}$ is the root of the equation $L(s)=0$ in the region [$\mathrm{Re}(s)<0$ and $\mathrm{Im}(s)<-\omega_e$].

From Eqs. (C1), (C2), and (C4), we can obtain the amplitudes (15) and (16) by setting $s=-y-i\omega_e$, where $m_2(s)=-iA_b(0)J+A_a(0)[s+i\omega_b+\beta(s)]$, $m_3(s)=-iA_a(0)J+A_b(0)[s+i\omega_a+\alpha(s)]$ and $m_4(s)=-iA_a(0)J+A_b(0)[s+i\omega_a+\beta(s)]$.

APPENDIX D: THE SOLUTION TO THE CUBIC EQUATION

The quantity p satisfies a cubic equation

$$p^3+bp^2+cp+d=0, \tag{D1}$$

with $b=-2\sqrt{\omega_e}$, $c=r$, $d=-c_e$. Its solutions can be found in any mathematics manual. If $B^2-4AC<0$ with $A=b^2-3c$, $B=bc-9d$, $C=c^2-3bd$. There are three different real roots,

$$\begin{aligned}
p_1&=\frac{-b-2\sqrt{A}\cos\theta}{3},\\
p_2&=\frac{-b+\sqrt{A}[\cos\theta-\sqrt{3}\sin\theta]}{3},\\
p_3&=\frac{-b+\sqrt{A}[\cos\theta+\sqrt{3}\sin\theta]}{3},
\end{aligned} \tag{D2}$$

where $\theta=\frac{1}{3}\arccos\left(\frac{2Ab-3B}{2\sqrt{A^3}}\right)$.

[1] D. E. Rourke, L. Khodarinova, and A. A. Karabanov, Phys. Rev. Lett. **92**, 163003 (2004).
[2] S. Gustavsson, F. Yan, J. Bylander, F. Yoshihara, Y. Nakamura, T. P. Orlando, and W. D. Oliver, Phys. Rev. Lett. **109**, 010502 (2012).
[3] E. Barnes and S. Das Sarma, Phys. Rev. Lett. **109**, 060401 (2012).
[4] A. J. Leggett, S. Chakravarty, A. T. Dorsey, M. P. A. Fisher, A. Garg, and W. Zwerger, Rev. Mod. Phys. **59**, 1 (1987).
[5] A. D. Greentree, C. Tahan, J. H. Cole, and L. C. L. Hollenberg, Nat. Phys. **2**, 856 (2006).
[6] J. R. Petta, A. C. Johnson, J. M. Taylor, E. Laird, A. Yacoby, M. D. Lukin, and C. M. Marcus, Science **309**, 2180 (2005).
[7] A. Wallraff, D. I. Schuster, A. Blais, L. Frunzio, R. S. Huang, J. Majer, S. Kumar, S. M. Girvin, and R. J. Schoelkopf, Nature (London) **431**, 162 (2004).
[8] P. Ao and J. Rammer, Phys. Rev. B **43**, 5397 (1991).
[9] A. Polyakov, Phys. Lett. B **72**, 224 (1977).
[10] A. Belitsky, V. Braun, A. Gorsky, and G. Korchemsky, Int. J. Mod. Phys. A **19**, 4715 (2004).
[11] S. Sachdev, *Quantum Phase Transitions* (Cambridge University Press, Cambridge, England, 1999).
[12] Y. Y. Zhang, Q. H. Chen, and K. L. Wang, Phys. Rev. B **81**, 121105(R) (2010).
[13] A. Alvermann and H. Fehske, Phys. Rev. Lett. **102**, 150601 (2009).
[14] F. Guinea, V. Hakim, and A. Muramatsu, Phys. Rev. B **32**, 4410 (1985).
[15] T. A. Costi and C. Kieffer, Phys. Rev. Lett. **76**, 1683 (1996).
[16] F. B. Anders, R. Bulla, and M. Vojta, Phys. Rev. Lett. **98**, 210402 (2007).
[17] S. Chakravarty and J. Rudnick, Phys. Rev. Lett. **75**, 501 (1995).
[18] J. T. Stockburger and C. H. Mak, Phys. Rev. Lett. **80**, 2657 (1998).
[19] K. Le Hur, P. Doucet-Beaupré, and W. Hofstetter, Phys. Rev. Lett. **99**, 126801 (2007).
[20] T. Zibold, E. Nicklas, C. Gross, and M. K. Oberthaler, Phys. Rev. Lett. **105**, 204101 (2010).
[21] M. A. Caprio, P. Cejnar, and F. Iachello, Ann. Phys. (NY) **323**, 1106 (2008).
[22] R. Silbey and R. A. Harris, J. Chem. Phys. **80**, 2615 (1984).
[23] H. Zheng, Eur. Phys. J. B **38**, 559 (2004).
[24] Z. Lü and H. Zheng, Phys. Rev. B **75**, 054302 (2007).
[25] A. W. Chin, Phys. Rev. B **76**, 201307(R) (2007).
[26] A. Winter, H. Rieger, M. Vojta, and R. Bulla, Phys. Rev. Lett. **102**, 030601 (2009).
[27] R. Bulla, N. H. Tong, and M. Vojta, Phys. Rev. Lett. **91**, 170601 (2003).
[28] M. Vojta, Phys. Rev. B **85**, 115113 (2012).
[29] N. H. Tong and M. Vojta, Phys. Rev. Lett. **97**, 016802 (2006).
[30] P. P. Orth, I. Stanic, and K. Le Hur, Phys. Rev. A **77**, 051601(R) (2008).
[31] A. Recati, P. O. Fedichev, W. Zwerger, J. von Delft, and P. Zoller, arXiv:cond-mat/0212413.
[32] K. Le Hur, Phys. Rev. Lett. **92**, 196804 (2004).
[33] K. Le Hur and M. R. Li, Phys. Rev. B **72**, 073305 (2005).

[34] H. B. Liu, J. H. An, C. Chen, Q. J. Tong, H. G. Luo, and C. H. Oh, Phys. Rev. A **87**, 052139 (2013).
[35] Q. J. Tong, J. H. An, H. G. Luo, and C. H. Oh, Phys. Rev. B **84**, 174301 (2011).
[36] Q. J. Tong, J. H. An, H. G. Luo, and C. H. Oh, Phys. Rev. A **81**, 052330 (2010).
[37] S. John and J. Wang, Phys. Rev. Lett. **64**, 2418 (1990).
[38] S. John and J. Wang, Phys. Rev. B **43**, 12772 (1991).
[39] G. Kweon and N. M. Lawandy, J. Mod. Opt. **41**, 311 (1994).
[40] S. John and T. Quang, Phys. Rev. A **50**, 1764 (1994).
[41] S. John, Phys. Rev. Lett. **58**, 2486 (1987).
[42] D. N. Zubariev, Sov. Phys. Usp. **3**, 320 (1960).
[43] G. D. Mahan, *Many Particle Physics*, 2nd ed. (Plenum, New York, 1990).
[44] H. Nakazato, M. Namiki, and S. Pascazio, Int. J. Mod. Phys. B **10**, 247 (1996).
[45] M. Miyamoto, Phys. Rev. A **72**, 063405 (2005).
[46] A. G. Kofman, G. Kurizki, and B. Sherman, J. Mod. Opt. **41**, 353 (1994).
[47] S. Y. Zhu, Y. P. Yang, H. Chen, H. Zheng, and M. S. Zubairy, Phys. Rev. Lett. **84**, 2136 (2000).
[48] Y. P. Yang, M. Fleischhauer, and S. Y. Zhu, Phys. Rev. A **68**, 022103 (2003).
[49] P. Y. Lo, H. N. Xiong, and W. M. Zhang, Sci. Rep. **5**, 9423 (2015).
[50] S. Pellegrin and G. Kurizki, Phys. Rev. A **71**, 032328 (2005).
[51] P. Ullersma, Physica **32**, 27 (1966).
[52] P. Ullersma, Physica **32**, 56 (1966).
[53] P. Ullersma, Physica **32**, 74 (1966).
[54] P. Ullersma, Physica **32**, 90 (1966).
[55] S. Bochner and K. Chandrasekharan, *Fourier Transforms* (Princeton University Press, Princeton, NJ, 1949).
[56] W.-M. Zhang, P.-Y. Lo, H.-N. Xiong, Matisse Wei -Yuan Tu, and F. Nori, Phys. Rev. Lett. **109**, 170402 (2012).
[57] P. Lodahl, A. F. van Driel, I. S. Nikolaev, A. Irman, K. Overgaag, D. Vanmaekelbergh, and W. L. Vos, Nature (London) **430**, 654 (2004).
[58] B. Bellomo, R. Lo Franco, S. Maniscalco, and G. Compagno, Phys. Rev. A **78**, 060302(R) (2008).
[59] W. K. Wootters, Phys. Rev. Lett. **80**, 2245 (1998).
[60] T. Yu and J. H. Eberly, Phys. Rev. Lett. **93**, 140404 (2004).
[61] H. Ollivier and W. H. Zurek, Phys. Rev. Lett. **88**, 017901 (2001).
[62] C. Z. Wang, C. X. Li, L. Y. Nie, and J. F. Li, J. Phys. B: At. Mol. Phys. **44**, 015503 (2011).
[63] F. F. Fanchini, T. Werlang, C. A. Brasil, L. G. E. Arruda, and A. O. Caldeira, Phys. Rev. A **81**, 052107 (2010).
[64] P. Zanardi and N. Paunković, Phys. Rev. E **74**, 031123 (2006).
[65] S. J. Gu, S. S. Deng, Y. Q. Li, and H. Q. Lin, Phys. Rev. Lett. **93**, 086402 (2004).
[66] T. A. Costi and R. H. McKenzie, Phys. Rev. A **68**, 034301 (2003).
[67] H. Zheng, Phys. Rev. B **50**, 6717 (1994); **61**, 1088 (2000).
[68] J. M. Bendickson, J. P. Dowling, and M. Scalora, Phys. Rev. E **53**, 4107 (1996).
[69] C. W. Wong, X. Yang, P. T. Rackic, S. G. Johnson, M. Qi, Y. Jeon, G. Barbastathis, and S. Kim, Appl. Phys. Lett. **84**, 1242 (2004).
[70] S. Foresi, P. R. Villeneuve, J. Ferrera, E. R. Thoen, G. Steinmeyer, S. Fan, J. D. Joannopoulos, L. C. Kimerling, H. I. Smith, and E. P. Ippen, Nature **390**, 143 (1997).
[71] R. Dicke, Phys. Rev. **93**, 99 (1954).
[72] A. V. Andreev, V. I. Emel'yanov, and Yu. A. Ill'inskii, *Cooperative Effects in Optics, Superradiance and Phase Transitions* (Institute of Physics, Bristol, 1993).
[73] J. D. Joannopoulos, *Photonic Crystals: Molding the Flow of Light* (Princeton University, Princeton, NJ, 2008).